EPJ B
Condensed Matter and Complex Systems
EPJ.org your physics journal

Eur. Phys. J. B (2017) 90: 221 DOI: 10.1140/epjb/e2017-80524-6

Periodic composites: quasi-uniform heat conduction, Janus thermal illusion, and illusion thermal diodes

Liujun Xu, Chaoran Jiang, Jin Shang, Ruizhe Wang, and Jiping Huang

edp sciences
Società Italiana di Fisica
Springer

Eur. Phys. J. B (2017) 90: 221
DOI: 10.1140/epjb/e2017-80524-6

THE EUROPEAN PHYSICAL JOURNAL B

Regular Article

Periodic composites: quasi-uniform heat conduction, Janus thermal illusion, and illusion thermal diodes

Liujun Xu[1], Chaoran Jiang[1], Jin Shang[1], Ruizhe Wang[1], and Jiping Huang[1,2,a]

[1] Department of Physics, State Key Laboratory of Surface Physics, and Key Laboratory of Micro and Nano Photonic Structures (MOE), Fudan University, Shanghai 200433, P.R. China
[2] Collaborative Innovation Center of Advanced Microstructures, Nanjing 210093, P.R. China

Received 14 September 2017 / Received in final form 21 September 2017
Published online 13 November 2017 –

Abstract. Manipulating thermal conductivities at will plays a crucial role in controlling heat flow. By developing an effective medium theory including periodicity, here we experimentally show that nonuniform media can exhibit quasi-uniform heat conduction. This provides capabilities in proposing Janus thermal illusion and illusion thermal rectification. For the former, we study, via experiment and theory, a big periodic composite containing a small periodic composite with circular or elliptic particles. As a result, we reveal the Janus thermal illusion that describes the whole periodic system with both invisibility illusion along one direction and visibility illusion along the perpendicular direction, which is fundamentally different from the existing thermal illusions for misleading thermal detection. Further, the Janus illusion helps to design two different periodic systems that both work as thermal diodes but with nearly the same temperature distribution, heat fluxes and rectification ratios, thus being called illusion thermal diodes. Such thermal diodes differ from those extensively studied in the literature, and are useful for the areas that require both thermal rectification and thermal camouflage. This work not only opens a door for designing novel periodic composites in thermal camouflage and heat rectification, but also holds for achieving similar composites in other disciplines like electrostatics, magnetostatics, and particle dynamics.

1 Introduction

Preventing or postponing the advent of energy crises is particularly important for human beings. The so-called energy crisis corresponds to the fact that energy sources like coal, petroleum, and natural gas become less and less due to the consumption. Nevertheless, in the duration, more and more thermal energy is produced and wasted. Thus, manipulating the transfer of thermal energy could be a reliable way for overcoming energy crises. Since thermal conductivities are the fundamental parameter describing the ability of a material to conduct heat, manipulating thermal conductivities at will is crucially important to control the flow of thermal energy.

It is known that both wave and diffusion are two important methods for transferring energy or matter, which are described by wave and diffusion equations, respectively. In contrast to wave equations [1–3], it is still far from being satisfactory to apply periodicity to design materials that are described by diffusion equations [4]. It is theoretically known that such nonuniform periodic structures exhibit uniform heat conduction when the mean size of nonuniformity (period of the structure) is much less than the mean size of the temperature change. But, to our knowledge, this has no direct experimental demonstration.

In this work, we shall develop an effective medium theory incorporating periodicity. As a result, we show, by experiment, that such periodicity can help a porous medium to exhibit almost the same temperature distribution and heat flux as that of a prearranged uniform medium surrounding the porous medium. The periodic porous medium actually corresponds to omnidirectional thermal invisibility because along any directions, one is unable to thermally distinguish the periodic porous medium from the uniform host medium by using thermal detection. Clearly, this kind of thermal invisibility is distinctly different from that based on cloaking [5–16], but it is somehow similar to the thermal transparency of a single multilayered sphere [17]; the cloaking [5–16] is mainly achieved by developing theories of coordinate transformation [18] or conformal mapping [19]. Further, the quasi-uniform heat conduction in nonuniform media with periodicity provides capabilities in proposing two new physical concepts: one is Janus thermal illusion, which serves as a new member (with new mechanism/behavior) of the family of the existing thermal illusions for misleading thermal detection [14,20–24]; the other is illusion thermal rectification, which owns "illusion" as an additional freedom of control, thus enriching the research on thermal rectification [25–27]. Our rectification may have potential applications in fields that require thermal rectification and thermal camouflage together.

[a] e-mail: jphuang@fudan.edu.cn

2 Theory

To proceed, we first develop a theory, following the effective medium theories for heat transfer [28–32]. Here we consider a two-dimensional binary composite, where many elliptic particles of thermal conductivity κ_1 and area fraction p are periodically embedded in a matrix of κ_2 and $1-p$. All the particles have their long (or short) axes aligned along x (or y) direction, whose shape factors characterizing the shape of the particles are L_i with $i = x$ or y along x or y direction. Here $L_x + L_y = 1$, and $L_x = L_y = 0.5$ for circular particles. Then we put this composite into an external thermal gradient field $\boldsymbol{\nabla} T_0$, and denote the local thermal gradient field inside the particle by $\boldsymbol{\nabla} T_1$, and that inside the matrix by $\boldsymbol{\nabla} T_2$. Solving the fundamental diffusion equation, namely the Laplace's equation $\boldsymbol{\nabla}^2 T = 0$ in thermodynamics with the following boundary conditions, where ξ describes the boundary of the elliptic particle

$$\begin{cases} T_1\,(r=0) \text{ is finite}, \\ T_2\,(r\to\infty) = \boldsymbol{\nabla} T_2 \cdot \boldsymbol{i}, \\ T_1\,(\xi) = T_2\,(\xi)\,, \\ -\kappa_1 \frac{\partial T_1}{\partial \xi}\big|_\xi = -\kappa_2 \frac{\partial T_2}{\partial \xi}\big|_\xi, \end{cases} \tag{1}$$

we can derive the following relationship

$$\boldsymbol{\nabla} T_1 = \frac{\kappa_2}{L_i \kappa_1 + (1-L_i)\kappa_2} \boldsymbol{\nabla} T_2. \tag{2}$$

Next, we calculate the area-averaged thermal gradient field $\langle \boldsymbol{\nabla} T \rangle \,(\equiv p \langle \boldsymbol{\nabla} T_1 \rangle + (1-p) \langle \boldsymbol{\nabla} T_2 \rangle)$ inside the composite which should be equal to the external thermal gradient field, $\langle \boldsymbol{\nabla} T \rangle = \boldsymbol{\nabla} T_0$. Here $\langle \cdots \rangle$ denotes the volume average of .... On the other hand, the effective thermal conductivity κ_e can be derived according to Fourier's law

$$\kappa_e = \frac{-\boldsymbol{J}}{\boldsymbol{\nabla} T_0} = \frac{-\boldsymbol{J}}{\langle \boldsymbol{\nabla} T \rangle}. \tag{3}$$

Then we obtain

$$\kappa_e = \frac{p\kappa_1 \langle \boldsymbol{\nabla} T_1 \rangle + (1-p)\,\kappa_2 \langle \boldsymbol{\nabla} T_2 \rangle}{p \langle \boldsymbol{\nabla} T_1 \rangle + (1-p) \langle \boldsymbol{\nabla} T_2 \rangle}, \tag{4}$$

where

$$\langle \boldsymbol{\nabla} T_1 \rangle = \frac{\kappa_2}{L_i \kappa_1 + (1-L_i)\kappa_2} \langle \boldsymbol{\nabla} T_2 \rangle. \tag{5}$$

Equation (5) is a direct result of equation (2) due to the distribution of the identical particles embedded in the manner of periodic array, and $L_i = \frac{ab}{2} \int_0^\infty \frac{\mathrm{d}s}{(i^2+s)\sqrt{(a^2+s)(b^2+s)}}$ where a and b are semi-axes of the elliptic particles (especially for circular particles, $a = b$).

Similarly, for a three-dimensional binary composite with many spherical particles periodically embedded in a matrix, equation (2) (for the two-dimensional system) should be replaced with

$$\boldsymbol{\nabla} T_1 = \frac{3\kappa_2}{\kappa_1 + 2\kappa_2} \boldsymbol{\nabla} T_2. \tag{6}$$

Then we achieve the effective thermal conductivity κ_e for the three-dimensional case on the same footing as equations (3)–(5). The resulting κ_e has the same mathematical expression as the Maxwell-Garnett theory in dielectrics [33–36], which justifies the derivation of equations (3)–(5) in two dimensions, at least to some extent. Certainly, the direct justification may resort to the following experimental comparison.

In what follows, all the particles mentioned above are only occupied by air, so that we could discuss the properties of the desired porous media. Naturally, the air can be replaced with other materials in order to achieve arbitrary values of κ_e.

3 Experiment

Then, we fabricate six samples; see Figures 1a–1f. The samples contain air, brass and phosphor copper, whose thermal conductivities are 0.026 W/(m·K), 109 W/(m·K) and 54 W/(m·K), respectively. Samples I and II are obtained according to the requirement of equations (4) and (5); either of them contains a middle square occupied by a porous medium (which contains air and brass) as a patch. For the sake of comparison, we also fabricate four other samples, namely, Samples III–VI. Sample III includes phosphor copper only, Sample IV involves the middle square with a random distribution of air in brass, Sample V's middle square is occupied by air only, and Sample VI's middle square has brass only. Then, based on the apparatus shown in Figure 1g, we use the thermal camera to detect the temperature distribution of the six samples. To be mentioned, the convection exists in our experiment. However, our samples have big thermal conductivities, which leads to the big heat flux. So the small heat loss resulting from convection can be neglected compared with the big heat flux. The measurement results are displayed in Figure 2. It is clear that both Sample I and Sample II possess nearly the same heat signatures as Sample III. This comparison indicates that the middle square of Sample I or II can work as a good thermal patch because it offers the specific heat signature as if the host materials (phosphor copper) were still located in the middle square of Sample I/II. In other words, according to the thermal detection as shown in Figures 2a–2c, people cannot distinguish Samples I–II's porous media (composed of air and brass in the middle square) from Sample III's phosphor copper located in the relevant middle square. So far, we can conclude that Figures 2a–2c display a special type of thermal invisibility, which is not only in-plane but also out-of-plane, thus being named as omnidirectional thermal invisibility. This thermal invisibility is fundamentally different from the invisibility based on cloaking [5–16]. Also importantly, because the middle squares of Figures 2a–2c have the same equivalent thermal conductivity according to equation (4), Fourier's law of

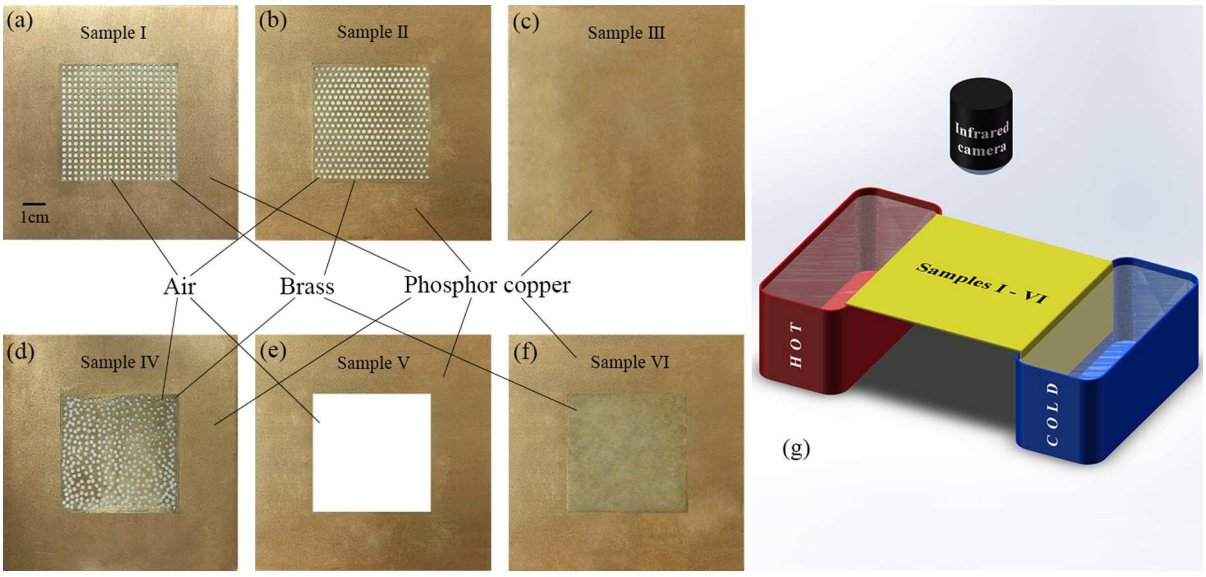

Fig. 1. (a–f) Six plate samples (Samples I–VI), each with size 10 cm × 10 cm and thickness 0.3 mm, fabricated for experimental measurement using the Flir E60 thermal camera based on (g) the experimental apparatus, where HOT and COLD denote the hot and cold source, respectively. (a, b, d–f) show a 5 cm × 5 cm middle square, out of which is occupied by phosphor copper; in (a and b), the middle square contains 400 air circles (with radius 0.5 mm) embedded in brass in the manner of (a) square lattice with lattice constants 0.25 cm × 0.25 cm and (b) centered rectangular lattice with lattice constants 0.24 cm × 0.48 cm; the middle squares of (d–f) include (d) 400 air circles randomly distributed in brass, (e) air, and (f) brass. The air circles occupying the middle squares of (a, b and d) have a radius of 0.8 mm and an area fraction of 33.76%. For comparison, (c) Sample III is made of homogeneous phosphor copper.

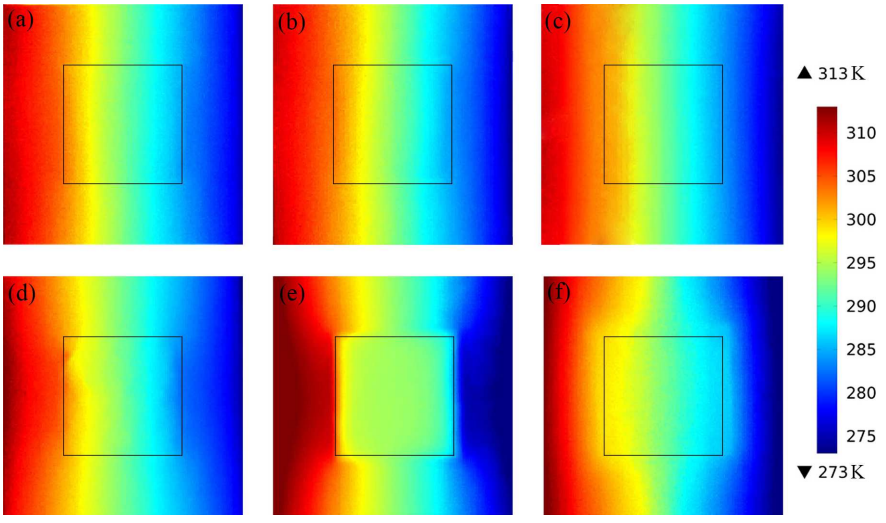

Fig. 2. Experimental measurement result of (a–f) Samples I–VI, which correspond to Figures 1a–1f, respectively. The color surface displays the distribution of temperature. The middle squares are added for the sake of comparison.

heat conduction helps us conclude that the middle squares of Figures 2a–2c have the same amount of heat flux as well. Besides the same temperature distribution, the same heat flux is another requirement of good thermal patch or omnidirectional thermal invisibility.

It is worth noting that the good agreement among Figures 2a–2c arise from the periodic array of air in Figures 2a and 2b. This point can be better understood by Figure 2d. In Figure 2d, we show the temperature distribution of the same air-brass medium, where the air is randomly distributed instead. Clearly, the random distribution of air in Figure 2d strongly affects the distribution of temperature either within the middle square or outside it. The failure of effective medium theory with a random structure can be understood from the following aspect. Our random structure is a finite system, so the randomness will lead to the fluctuation of thermal conductivity. Especially when the area fraction is big, random particles may get connected, which will cause the decrease of thermal conductivity. So the real thermal conductivity may be

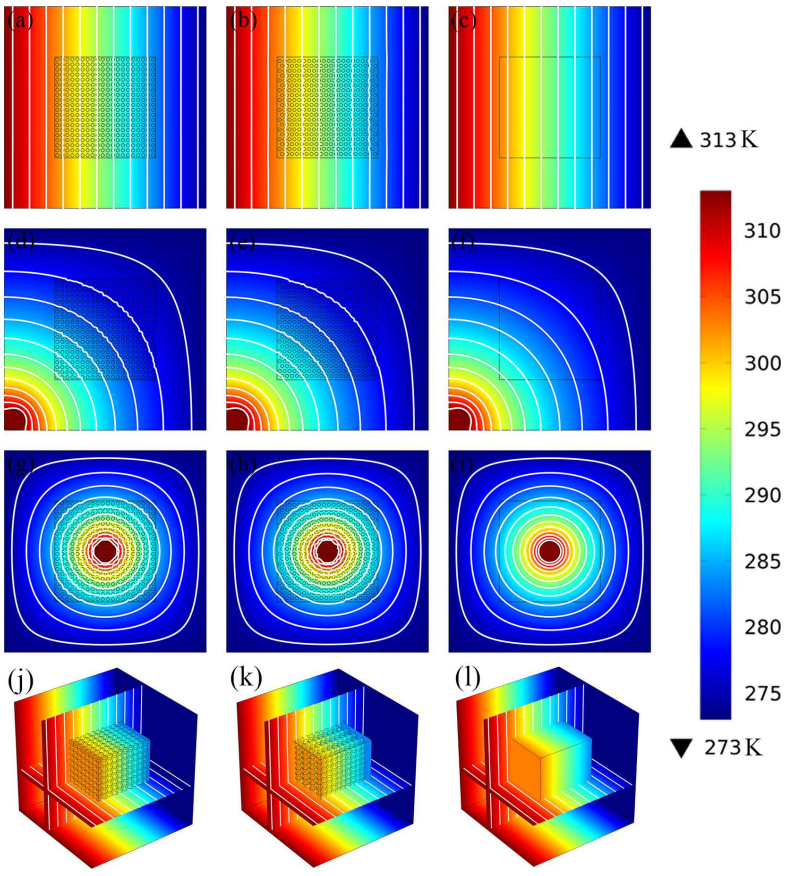

Fig. 3. Temperature distribution obtained by finite-element simulations: the white lines represent isotherms. (a–c) show the respective two-dimensional result of Samples I–III for line hot/cold sources, where the upper or lower boundary is set at heat insulation; (d–f) are same as (a–c), but for a point hot source with radius 5 mm located in the bottom-left corner, where the left or lower boundary is set at heat insulation and the upper or right boundary is kept at 273 K; (g–i) are also same as (a–c), but the same point hot source is located in the center instead, where the four boundaries remain 273 K. (j–l) are same as (a–c), respectively, but for three dimensions 10 cm × 10 cm × 10 cm: the middle cube has a size of 5 cm × 5 cm ×5 cm; this cube in (j and k) involves 1000 air spheres with volume fraction 40.46% and radius 2.3 mm each, which are assembled in the structure of (j) a simple cubic lattice with lattice constants 0.5 cm × 0.5 cm × 0.5 cm and (k) a body-centered tetragonal lattice with lattice constants 0.47 cm × 0.47 cm × 0.94 cm. For clarity, we mark out air circles in (a, b, d, e, g and h) and air spheres in (j and k).

different from the theoretical value in random structure. On the contrary, there is no fluctuation in periodic structure, so the real thermal conductivity agrees well with the theoretical value. This helps to reveal the role of periodic arrays in achieving the above-mentioned omnidirectional thermal invisibility as shown in Figures 2a and 2b.

Additionally, we fill the middle square with air or brass; see Figures 2e and 2f. Because of the low (high) conductivity of air (brass), the temperature distribution is affected significantly. Figures 2e and 2f also helps to prove the good agreement among Figures 2a–2c, at least to some extent.

4 Computer simulation and experiment

In order to well understand Figures 2a–2c of Samples I–III, we also perform the finite-element simulations based on the commercial software COMSOL Multiphysics (https://www.comsol.com/). Results are shown in Figures 3a–3c that are similar to Figures 2a–2c, respectively. In Figures 3a–3c, the isothermal lines make the comparison more clear, confirming the afore-mentioned results of Figures 2a–2c in the main text. Incidently, the tiny wiggle in the middle square of Figure 3b has a characteristic length that is same as the lattice constant. For the sake of generality, we also plot Figures 3d–3l. Details are as follows. Figures 3d–3f show the case of a point source located outside the middle square. Clearly, Figures 3d and 3e also show a good thermal patching effect, namely, the middle square exhibits the same temperature distribution and heat flux as if the host material (outside the middle square) were located in the middle square. The same conclusion can be drawn for Figures 3g–3i where the point heat source is put at the center of the middle square. All Figures 3a–3i focus on the plate or surface in two dimensions. As mentioned, good thermal patching effects come to appear for such cases. Actually, all the above discussions on good thermal patching effects or omnidirectional thermal invisibility in two dimensions can be extended

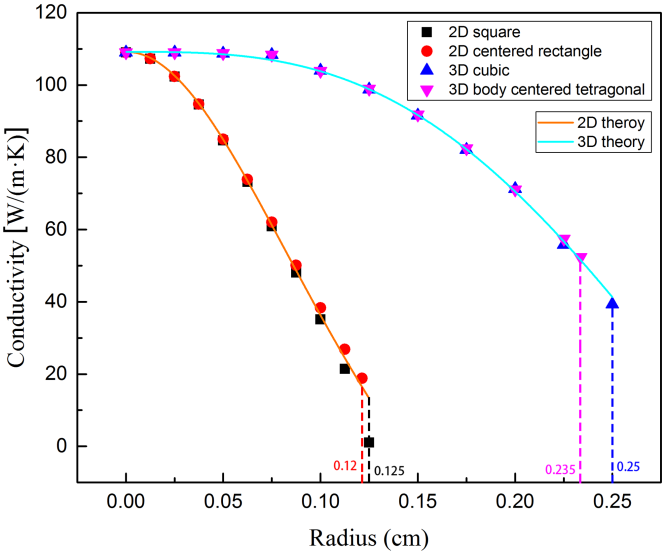

Fig. 4. Effective conductivity of the middle square/volume versus the radius of air circles/spheres: the two solid lines are results calculated from equation (3) for two dimensions ("2D theory") and three dimensions ("3D theory"); four kinds of symbols are results obtained from finite-element simulations for two dimensions ("2D square" and "2D centered rectangle") and three dimensions ("3D cubic" and "3D body centered tetragonal"). "2D square" ("2D centered rectangle") corresponds to the middle square shown in Figure 1a [Fig. 1b], but the radius of the air circles changes from 0 to the maximum 0.125 cm (0.12 cm) corresponding to $p = 78.54\%$ ($p = 72.38\%$); "3D cubic" ("3D body centered tetragonal") denotes the middle volume shown in Figure 3j [Fig. 3k], but the radius of the air spheres varies from 0 to the maximum 0.25 cm (0.235 cm) accompanied by $p = 52.36\%$ ($p = 43.49\%$). It is shown that the theory based on equation (3) agrees well with the finite element simulations.

to three dimensions; see Figures 3j–3l. Figures 3j and 3k have a middle cube of air and brass, indicating also the same heat signature (namely, temperature distribution and heat flux) as that in Figure 3l that contains the pure phosphor copper only.

In the above analysis [Figs. 1a, 1b and 1d and 2a, 2b and 2d], equations (4) and (5) have been used to determine the values of air's area fraction p that is proportional to the radius of air circles. In practice, to guarantee the periodic structure of the porous medium for patching a specific host material (say, the phosphor copper used herein), the p (or radius of air circles) needs to be tuned accordingly if one adopts different matrices in the middle square/cube. In this case, equation (4) can still help to predict the effective conductivity of the middle square as a function of the radius (or p) of air circles; see Figure 4. Figure 4 displays that the effects of increasing radius on reducing the effective thermal conductivity are same for different lattices in two or three dimensions. This also explains the good agreement between Figures 2a–2c and Figures 3a–3c. Figure 4 also shows that a periodic composite with arbitrary thermal conductivities can be obtained by choosing parameters appropriately.

In fact, the above findings could be more useful. For example, we fabricate three additional experimental samples, Samples VII–IX; see Figures 5a1–5d1 to realize Janus illusion. Janus is a mythological character in Greek, which is often used to describe two distinct properties. Here we demonstrate the invisible illusion in one direction and visible illusion in the perpendicular one, and thus we give the two distinct illusion a name as Janus illusion. The core of Janus illusion is to keep the same effective thermal conductivity of the same direction through careful calculation from equations (4) and (5). The hot (cold) heat bath is at the left (right) end in Figures 5a2–5a4 and 5b2–5b4, and at the top (bottom) end in Figures 5c2–5c4 and 5d2–5d4. Then we use the Flir E60 thermal camera with a resolution of 0.1 K to detect the temperature distribution of the samples; see Figures 5a2–5d2.

Figure 5a2 shows that the middle square region of Sample VII does not affect the distribution of temperature outside this region, thus yielding invisibility. Or, alternatively we may call this middle square region as an invisible region. In addition, the middle square region of Sample VII [Fig. 5a2] has the same thermal image as that of Sample VIII [Fig. 5b2]. Namely, the two middle square regions of Samples VII and VIII cannot be distinguished by using thermal detection, thus leading to illusion. In this regard, we may conclude that Sample VII has a kind of invisibility illusion for the horizontal temperature gradient.

On the other hand, Figure 5c2 displays that the middle square region of Sample VII can affect the temperature distribution outside this region indeed, which causes visibility. Additionally, the middle square region of Sample VII [Fig. 5c2] owns the same thermal image as the middle square region of Sample VIII [Fig. 5d2]. Namely, the two middle square regions of Samples VII and IX can not be separated according to the thermal measurement, which leads to illusion. In this sense, we may say that Sample VII has a type of visibility illusion for the vertical temperature gradient.

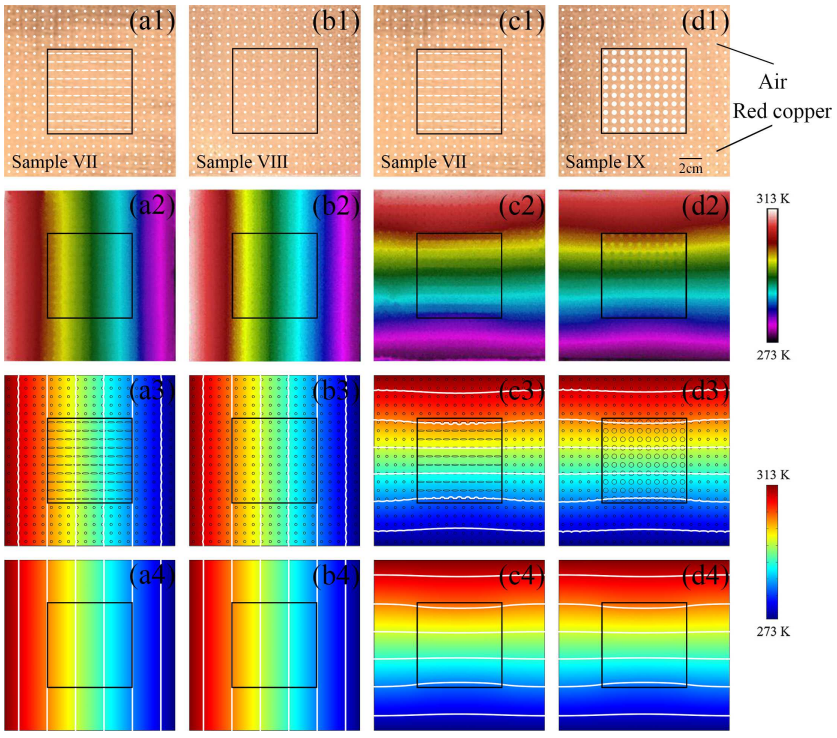

Fig. 5. Janus thermal illusion: (a1–d2) experimental and (a3–d4) simulation results; the color surface in (a2–d4) denotes the temperature distribution, and the white lines in (a3–d4) represent the isotherms. (a1–d1) show three experimental samples, (a1 and c1) Sample VII, (b1) Sample VIII and (d1) Sample IX, each with size 15 cm × 15 cm and thickness 0.3 mm. In (a1–d1), we mark out a middle square with size 7.5 cm × 7.5 cm, out of which is occupied by the same red copper with conductivity 397 W/(m·K) drilled with 300 air circular holes with 0.026 W/(m·K) and radius 0.11 cm in a periodic array. The middle square of (a1 and c1) Sample VII possesses the same red copper, but drilled with 100 air elliptic holes in a periodic manner, whose major (or minor) semi-axis is 0.3 cm (or 0.06 cm) with shape factor 1/6 (or 5/6) along the semi-axis; the middle square of (b1) Sample VIII is drilled with 100 air circular holes with radius 0.11 cm, and thus the whole (b1) Sample VIII is a periodic composite with a fixed lattice constant; the middle square of (d1) is drilled with 100 air circular holes with radius 0.21 cm. (a2–d2) are experimental measurements corresponding to (a1–d1), respectively. (a3–d3) are simulation results corresponding to (a1–d1), respectively. (a4–d4) are simulation results for materials with effective conductivities determined by equation (3) according to the structure shown in (a1)–(d1), respectively: outside the middle square is the material with conductivity 350 W/(m·K); the middle square in (a4) or (c4) is occupied by material with conductivity tensor diag (350, 238) W/(m·K); the middle square in (b4) or (d4) contains material with 350 W/(m·K) or 238 W/(m·K), respectively.

In a word, for the single Sample VII, it may own both invisibility illusion along the horizontal direction and visibility illusion along the vertical direction, and thus we call this kind of illusion as Janus illusion. The behavior of Janus illusion is also confirmed by finite element simulations [Figs. 5a3–5d3] and calculations [Figs. 5a4–5d4]. Further, the Janus illusion can help to propose illusion thermal diodes. See Figures 6a and 6d: when the hot heat bath is at the left end of the structure, the diodes allow heat conduction from left to right [Figs. 6b and 6e]; while it is at the right end, the diode prevent the heat conduction from right to left [Figs. 6c and 6f]. Although the diode in Figure 6a has a different periodic structure from that in Figure 6d, both of them possess almost the same temperature distribution, heat flux distribution, and rectification ratio [Figs. 6b, 6c, 6e and 6f]. Thus we call them "illusion diodes". Here, the diode is based on Peyrard's design principle [26] on thermal rectifier by using two segment materials whose temperature-dependence thermal conductivity behaviors are different. But, we design this kind of diodes to possess "illusion" as an additional freedom of control, which have potential applications in fields that require both thermal camouflage and thermal rectification.

5 Conclusion

To sum up, by developing an effective medium theory with periodicity, we have experimentally shown the quasi-uniform heat conduction in nonuniform media with periodicity. This heat conduction has helped to propose two new physical concepts, namely Janus thermal illusion and illusion thermal rectification. Our work not only opens a door for designing novel periodic composites in thermal camouflage and heat rectification, but also holds for achieving similar composites in other disciplines like electrostatics, magnetostatics and particle dynamics, where electric conductivities, magnetic permeabilities and diffusion coefficients respectively play the same role as thermal conductivities in thermotics.

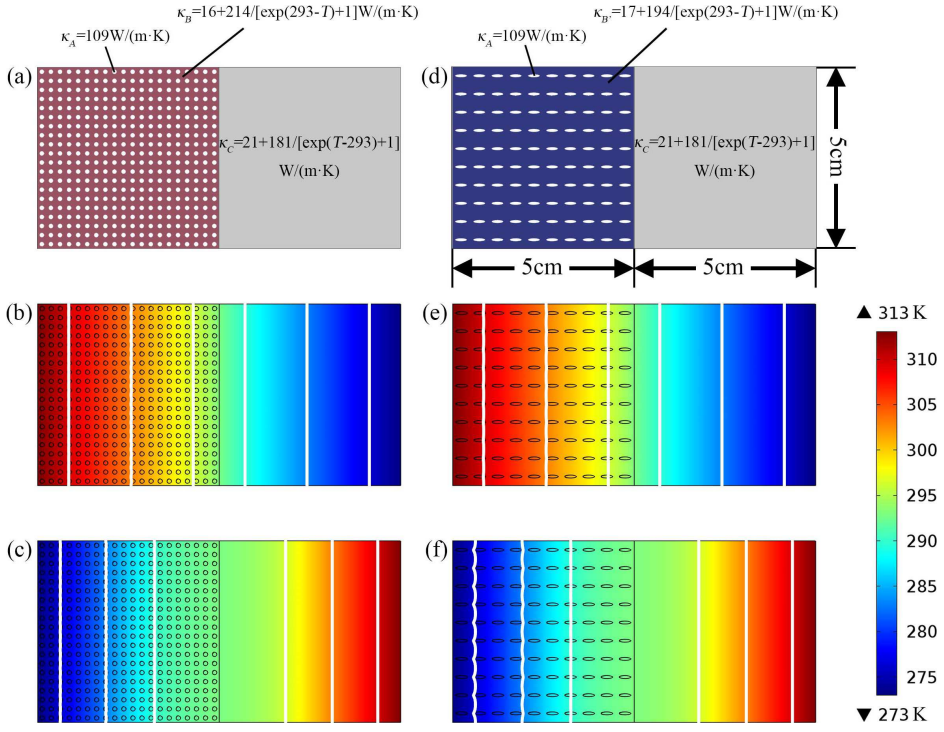

Fig. 6. Illusion thermal rectification based on periodic structure: simulation results. (a) is schematic graph showing the diode structure, where the left part made up of a host material B (with a temperature-dependent thermal conductivity, which may be realized with the aid of shape memory alloy according to the design proposed in Ref. [15]) containing 20×20 periodic circular holes occupied by material A with area fraction 18.1%. (b) is the distribution of temperature (color surface) and isotherms (white lines) in the thermal diode for high flux J_h. (c) is the same as (b), but the positions of the heat source and cold source are exchanged, thus showing the case of low flux J_l. (d) is schematic graph showing the illusion diode structure corresponding to (a). The difference is that there exist 10×10 periodic elliptic particles (area fraction 8.0%). (e) and (f) show the results of the diode in (d). (b) and (e) indicate the high heat flux: (b) $J_h = 7.84 \times 10^4$ W/m^2 and (e) $J_h = 7.83 \times 10^4$ W/m^2. (c) and (f) represent the low heat flux: (c) $J_l = 1.11 \times 10^4$ W/m^2 and (f) $J_l = 1.10 \times 10^4$ W/m^2. Thus, we obtain the rectification ratio, $(J_h - J_l) / (J_h + J_l)$, as 75.20% for (a) and 75.36% for (d). Parameters (thermal conductivities and sizes) are indicated in (a and d).

We thank Prof. H. Zhao and Dr. G. Wang for useful discussions. We acknowledge the financial support by the Science and Technology Commission of Shanghai Municipality under Grant No. 16ZR1445100, by Fudan's Undergraduate Research Opportunities Program, and by the National Fund for Talent Training in Basic Science (No. J1103204).

Author contribution statement

All the authors were involved in the preparation of the manuscript. All the authors have read and approved the final manuscript. J.H. and L.X. designed research; L.X., C.J., J.S., and R.W. performed research; L.X., C.J., J.S., R.W., and J.H. analyzed data; and L.X., C.J., J.S., R.W., and J.H. wrote the paper.

References

1. E. Yablonovitch, Phys. Rev. Lett. **58**, 841 (1987)
2. M.M. Sigalas, E.N. Economou, J. Sound Vibr. **158**, 382 (1992)
3. M. Maldovan, Phys. Rev. Lett. **110**, 025902 (2013)
4. G.Q. Gu, K.W. Yu, J. Phys. D: Appl. Phys. **30**, 1523 (1997)
5. C.Z. Fan, Y. Gao, J.P. Huang, Appl. Phys. Lett. **92**, 251907 (2008)
6. T. Chen, C.-N. Weng, J.-S. Chen, Appl. Phys. Lett. **93**, 114103 (2008)
7. S. Narayana, Y. Sato, Phys. Rev. Lett. **108**, 214303 (2012)
8. S. Guenneau, C. Amra, D. Veynante, Opt. Express **20**, 8207 (2012)
9. R. Schittny, M. Kadic, S. Guenneau, M. Wegener, Phys. Rev. Lett. **110**, 195901 (2013)
10. T.C. Han, T. Yuan, B.W. Li, C.W. Qiu, Sci. Rep. **3**, 1593 (2013)
11. H.Y. Xu, X.H. Shi, F. Gao, H.D. Sun, B.L. Zhang, Phys. Rev. Lett. **112**, 054301 (2014)
12. T.C. Han, X. Bai, D.L. Gao, J.T.L. Thong, B.W. Li, C.W. Qiu, Phys. Rev. Lett. **112**, 054302 (2014)
13. Y.G. Ma, Y.C. Liu, M. Raza, Y.D. Wang, S.L. He, Phys. Rev. Lett. **113**, 205501 (2014)
14. T.C. Han, X. Bai, J.T.L. Thong, B.W. Li, C.W. Qiu, Adv. Mater. **26**, 1731 (2014)
15. Y. Li, X.Y. Shen, Z.H. Wu, J.Y. Huang, Y.X. Chen, Y.S. Ni, J.P. Huang, Phys. Rev. Lett. **115**, 195503 (2015)

16. X.Y. Shen, Y. Li, C.R. Jiang, J.P. Huang, Phys. Rev. Lett. **117**, 055501 (2016)
17. X. He, L.Z. Wu, Phys. Rev. E **88**, 033201 (2013)
18. J.B. Pendry, D. Schurig, D.R. Smith, Science **312**, 1780 (2006)
19. U. Leonhardt, Science **312**, 1777 (2006)
20. X. He, L.Z. Wu, Appl. Phys. Lett. **105**, 221904 (2014)
21. N.Q. Zhu, X.Y. Shen, J.P. Huang, AIP Adv. **5**, 053401 (2015)
22. T.Z. Yang, X. Bai, D.L. Gao, L.Z. Wu, B.W. Li, J.T.L. Thong, C.W. Qiu, Adv. Mater. **27**, 7752 (2015)
23. T.Z. Yang, Y.S. Su, W.K. Xu, X.D. Yang, Appl. Phys. Lett. **109**, 121905 (2016)
24. Q.W. Hou, X.P. Zhao, T. Meng, C.L. Liu, Appl. Phys. Lett. **109**, 103506 (2016)
25. B. Li, L. Wang, G. Casati, Phys. Rev. Lett. **93**, 184301 (2004)
26. M. Peyrar, EPL **76**, 49 (2006)
27. N.B. Li, J. Ren, L. Wang, G. Zhang, P. Hänggi, B.W. Li, Rev. Mod. Phys. **84**, 1045 (2012)
28. P.G. Klemens, High Temp.-High Press. **23**, 241 (1991)
29. K.W. Schlichting, N.P. Padture, P.G. Klemens, J. Mater. Sci. **36**, 3003 (2001)
30. P.G. Klemens, M. Gell, Mater. Sci. Eng. A **245**, 143 (1998)
31. L. Braginsky, V. Shklover, G. Witz, H.-P. Bossmann, Phys. Rev. B **75**, 094301 (2007)
32. L. Braginsky, V. Shklover, Phys. Rev. B **78**, 224205 (2008)
33. J.P. Huang, K.W. Yu, Phys. Rep. **431**, 87 (2006)
34. L. Dong, J.P. Huang, K.W. Yu, G.Q. Gu, Eur. Phys. J. B **48**, 439 (2005)
35. Y.Y. Li, N.B. Li, B.W. Li, Eur. Phys. J. B **182**, 182 (2015)
36. L. Gao, L.P. Gu, Z.Y. Li, Phys. Rev. E **68**, 066601 (2003)